3D PRINTING

Self-assembled micro-organogels for 3D printing silicone structures

Christopher S. O'Bryan,[1] Tapomoy Bhattacharjee,[1] Samuel Hart,[1] Christopher P. Kabb,[2] Kyle D. Schulze,[1] Indrasena Chilakala,[1] Brent S. Sumerlin,[2] W. Gregory Sawyer,[1,3] Thomas E. Angelini[1,4]*

The widespread prevalence of commercial products made from microgels illustrates the immense practical value of harnessing the jamming transition; there are countless ways to use soft, solid materials that fluidize and become solid again with small variations in applied stress. The traditional routes of microgel synthesis produce materials that predominantly swell in aqueous solvents or, less often, in aggressive organic solvents, constraining ways that these exceptionally useful materials can be used. For example, aqueous microgels have been used as the foundation of three-dimensional (3D) bioprinting applications, yet the incompatibility of available microgels with nonpolar liquids, such as oils, limits their use in 3D printing with oil-based materials, such as silicone. We present a method to make micro-organogels swollen in mineral oil, using block copolymer self-assembly. The rheological properties of this micro-organogel material can be tuned, leveraging the jamming transition to facilitate its use in 3D printing of silicone structures. We find that the minimum printed feature size can be controlled by the yield stress of the micro-organogel medium, enabling the fabrication of numerous complex silicone structures, including branched perfusable networks and functional fluid pumps.

INTRODUCTION

Swollen microscale particles made from cross-linked polymers, generally known as microgels, have extremely useful rheological properties and are produced industrially as additives in personal care products, lubricants, coatings, and oil recovery fluids (*1*–*4*). A distinct behavior emerges with microgels when the particles are larger than 1 μm and tightly packed together (*5*). In contrast to traditional shear-thinning complex fluids composed of polymers or micelles, this packed bath of granular microgels transforms from a stable solid state into a flowing fluid phase when large external forces cause the granular gel particles to rearrange, which does not happen spontaneously under thermal forces. This transition is known as unjamming and occurs when externally applied stress exceeds a threshold value called the yield stress (*6*–*10*). Microgels are most often synthesized, swelled, and used in aqueous solvents, limiting their breadth of potential application; traditional microgel synthesis routes in organic solvents remain challenging and mostly limited to coating technologies (*1*, *2*). Thus, alternative and effective methods of producing granular-scale microgels in nonpolar solvents and oils will open untapped areas of technological application.

In one recently developed application area, jammed microgels are used to three-dimensionally (3D) print hydrogel and silicone structures, as well as living cell constructs (*11*, *12*). With this technique, printed material is physically trapped in space by packed microgels, which temporarily fluidize under the stress generated by a translating injection tip and then rapidly return to a jammed solid state (*8*–*10*). The jammed microgel material enables 3D printing of soft matter through its low modulus, low yield stress, localized yielding behavior, spontaneous reflow after yielding, and rapid recovery of elasticity. These properties facilitate 3D printing with a high degree of precision and control with aqueous soft materials. By contrast, demonstrations of silicone printing into microgel supports show that major challenges remain for nonaqueous soft materials. Interfacial interactions between silicone inks and aqueous support materials limit printing precision and inhibit adhesion between printed features (*13*); commercially available silicone-based microgels practically offer no rheological control of the support medium (*12*).

Silicone elastomer can be formulated to have low elastic modulus, high extensibility and toughness, excellent thermal and oxidative stability, and chemical inertness (*14*–*16*). Although this combination of properties has enabled a multitude of industrial uses to be developed for solid silicone elastomer, the challenges of handling viscous liquid silicone before curing limit its use in advanced additive manufacturing (*17*–*21*). 3D printing with industrially relevant nonpolar inks such as silicone would be greatly enhanced if a nonpolar jammed microgel system was available; a versatile, oil-based, jammed microgel material with rheological properties that can be tuned to mimic aqueous microgels would enable the precise 3D printing of silicones and organic soft materials by eliminating deleterious interfacial instabilities between printed materials and their microgel support.

Here, we develop a granular organic microgel system and demonstrate its use as an oil-based 3D printing support medium. The organogel particles are formed through the self-assembly of diblock and triblock copolymers dispersed at low concentration in mineral oil, in contrast to traditional polymerization routes to synthesizing microgels (*1*, *2*). Our granular organogel system has the rheological properties needed for precision 3D printing applications, including a low modulus (100 Pa), a low yield stress (3 to 4 Pa), and a short period for elastic recovery (1 s). 3D printing is performed by translating an injection needle through the organogel medium while depositing features made from numerous silicone-based materials. We investigate the interfacial instability between printed silicone features and the organogel support material, determining the limits of precision dictated by the balance of interfacial tension, yield stress, and feature size. We find that silicone features as small as 80 μm can be printed and remain indefinitely stable without cross-linking. We also find that the breakup of unstable features can be delayed markedly by increasing the viscosity of silicone inks,

[1]Department of Mechanical and Aerospace Engineering, University of Florida, Gainesville, FL 32611, USA. [2]Department of Chemistry, University of Florida, Gainesville, FL 32611, USA. [3]Department of Materials Science and Engineering, University of Florida, Gainesville, FL 32611, USA. [4]J. Crayton Pruitt Family Department of Biomedical Engineering, University of Florida, Gainesville, FL 32611, USA.
*Corresponding author. Email: t.e.angelini@ufl.edu

allowing even higher-precision (30 μm) structures to be manufactured. We demonstrate the capabilities of this method by creating 3D scaffolds, model tracheal implants, a perfusable 3D branched network, and a functional fluid pump.

RESULTS

Block copolymer self-assembly and rheology

Block copolymer self-assembly is a well-established route for designing soft materials, offering control of nanostructure and rheological properties (*22*–*24*). To formulate an organic microgel medium, we leverage this high degree of control provided by block copolymers, using a polystyrene-*block*-ethylene/propylene (SEP) diblock copolymer and a polystyrene-*block*-ethylene/butylene-*block*-polystyrene (SEBS) triblock copolymer. These polymers are assembled at low concentration [4 to 5 weight % (wt %)] in light mineral oil, a solvent selective for the ethylene-containing blocks (see Materials and Methods and Fig. 1A). The SEP diblock and SEBS triblock copolymers both self-assemble into structures with 1- to 2-nm glassy polystyrene cores and with coronas containing the oil-soluble blocks (*24*–*26*). In the pure triblock system, neighboring polystyrene cores are connected by bridges of ethylene/butylene blocks, resulting in a macroscopic network (*27*, *28*). The bridged polystyrene cores are analogous to the cross-links in more traditional formulations of aqueous microgels. The size of each polystyrene core is determined by the polystyrene length and mass density, whereas the spacing between cores is driven by the swelling of the oil-soluble block. In contrast to the pure triblock material, a suspension of discrete micelles is formed when only diblock copolymers are assembled. For both the triblock and diblock systems, the glassy polystyrene cores prevent the exchange of polymers between structures.

Previous work shows that fluid instabilities are overcome by 3D printing into a self-healing, jammed solid made from polymer microgels at low polymer concentration (*11*, *12*, *29*). Here, 3D printing into the diblock micelle suspension is inhibited by its fluid-dominated rheology; printed features will move under buoyancy forces or break up into droplets (Fig. 1, B and C). By contrast, 3D printing into the triblock network is inhibited by its solid properties; while the cross-linked network can support structures, the printing nozzle severs polymer bridges as it travels through the printing medium, irreversibly damaging the gel (Fig. 1, D and E). To create a solid material that can support printed structures and that is not damaged by a translating printing nozzle, we blend the diblock and triblock copolymers in search of a formulation having insufficient bridging to create a system-spanning network, but having enough bridging to create microscale organogels (Fig. 1, F to H). The addition of diblock copolymers promotes gel swelling without creating bridges. This micro-organogel system should fluidize at the location of applied stress and rapidly resolidify upon the removal of stress, much like the behavior of aqueous microgels, allowing for the precise manufacture of 3D-printed silicone structures.

To identify a formulation with favorable rheological properties for silicone 3D printing, we perform several types of rheological measurement on samples with different diblock and triblock copolymer ratios and various global polymer concentrations. To classify a given formulation as solid or liquid, we conduct a frequency sweep at low strain amplitude (1%), measuring the elastic and viscous shear moduli (Fig. 2A). To identify the yield stress of the material, we measure stress under unidirectional shear at different shear rates. In these data, the yield stress corresponds to the plateau in shear stress at low shear rate. Yield stress is determined by fitting the Herschel-Bulkley model to the data, given by $\sigma = \sigma_y + k\dot{\varepsilon}^n$, where σ is the measured stress, σ_y is the yield stress, and $\dot{\varepsilon}$ is the applied shear rate (Fig. 2B) (*30*, *31*). Finally, we determine the rate of elastic recovery in the material after the removal of applied shear stress. This thixotropic time is the duration over which shear rate drops to 0 after a high level of applied shear stress is rapidly removed (Fig. 2C). A short thixotropic time improves 3D printing performance because it reduces the duration over which the microgel support material is fluidized and mechanically unstable.

We find that a formulation of 4.5 wt % global polymer concentration with an equal incorporation of diblock and triblock copolymers (that is, 1:1 wt %) has the rheological properties consistent with jammed microgels and needed for precise 3D printing of silicone (see the Supplementary Materials). The frequency-dependent elastic and viscous shear moduli of the 50:50 mixture are relatively flat and fully separated across a wide frequency range, exhibiting an elastic modulus of about 100 Pa. This formulation has a yield stress of 3 to 4 Pa and a thixotropic time of about 1 s (see the Supplementary Materials for further rheological characterization). This combination of rheological behaviors is the fingerprint of jammed soft granules. To test whether this formulation produces micro-organogels, we dilute the sample with mineral oil and collect optical micrographs using phase-contrast illumination. We observe 2- to 4-μm granular structures (Fig. 2D and movie S1). Using small-angle x-ray scattering (SAXS) to measure the spacing of polystyrene cores, in combination with stoichiometric calculations, we find that within the pure triblock network phase, each polystyrene core is connected to its neighbors through an average of 12 bridges. In the microgel phase, each polystyrene core only connects through an average of six bridges. It is intriguing that the organo-microgels formulated here self-assemble when the coordination number between polystyrene cores lies at the limit of the Maxwell criterion for the stability of solids (see the Supplementary Materials) (*32*).

The rheological behavior of this copolymer system can be tuned; as the concentration of the triblock polymer is increased relative to the diblock polymer, the yield stress and modulus of the gel increase (Fig. 2A). Unrecoverable yielding of the 100% triblock material is observed in shear rate sweeps; when the applied shear stress exceeds the yield stress of the gel, SEBS triblock bridges are severed (Fig. 2B). Conversely, materials with high diblock proportions behave like non-Newtonian liquids, exhibiting a crossover of elastic and viscous shear moduli in frequency sweep measurements and having no observed yield stress in shear rate sweeps (Fig. 2, A and B). In the 50:50 formulation that forms microgels, we find that the rheological properties of the gel remain relatively unchanged up to a temperature of 50°C. At 60°C and above, the material is dominantly fluid-like (see the Supplementary Materials). The moduli and the yield stress of the different formulations can also be controlled by changing the global polymer concentration (see the Supplementary Materials).

Printing, precision, stability, and strength

Printing of silicone elastomers into the organogel support medium is accomplished using a custom-made 3D printer consisting of a modified linear stage as a syringe pump attached to three linear translation stages (movie S2). The three linear translation stages follow a predetermined trajectory at a specified translation speed, whereas the syringe pump continuously deposits the silicone elastomer into the organogel medium at a set flow rate (see Materials and Methods). To test the level of control provided by the micro-organogel for silicone 3D printing, we create a series of linear features at many different combinations of nozzle translation speed (0.1 to 10 mm/s) and injection flow rate (10 to 10,000 μl/hour). A

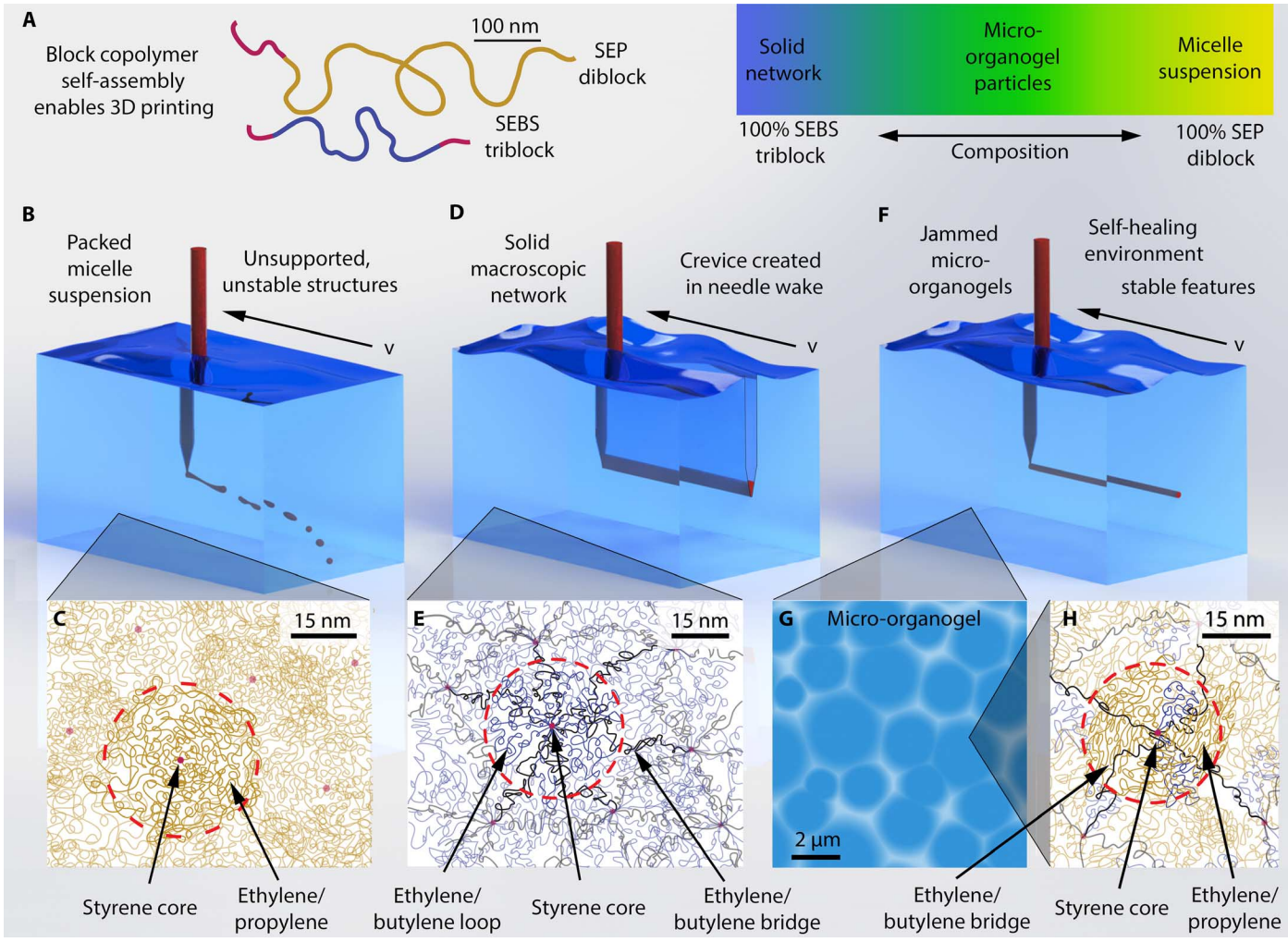

Fig. 1. Block copolymer self-assemblies and micro-organogels. (**A**) Organogel support materials are formulated with light mineral oil, polystyrene-*block*-polyethylene/propylene diblock copolymers, and polystyrene-*block*-polyethylene/butylene-*block*-polystyrene triblock copolymers (polymers drawn are extended to illustrate their contour lengths). (**B**) High concentrations of diblock copolymers result in a fluid phase of packed micelles, unable to support printed structures. (**C**) Diblock micelles consist of polystyrene cores (red dots) surrounded by ethylene/propylene coronas. (**D**) At high concentrations of triblock copolymers, the support bath becomes globally cross-linked, and the printing nozzle causes permanent damage as it moves across the gel. (**E**) Ethylene/butylene midblocks assemble either into cross-link "bridges," in which the polystyrene endblocks are found in different cores, or into "loops," in which both polystyrene endblocks are located in the same core. (**F** and **G**) An equal blend of diblock and triblock copolymers results in closely packed microgels. Packed microgels provide a self-healing environment, allowing a printing nozzle to repeatedly transverse the same region while simultaneously supporting printed structures. (**H**) The micro-organogels form when the diblock copolymers replace the triblock copolymers, reducing the number of ethylene/butylene bridges that form until the material is no longer a continuous network.

test ink is made from a vinyl-terminated polydimethylsiloxane (PDMS) polymer, mixed with a (mercaptopropyl)methylsiloxane-dimethylsiloxane copolymer cross-linking agent at a 3:1 ratio (see Materials and Methods). To enable 3D imaging with a laser scanning fluorescence confocal microscope, fluorescent beads are dispersed in the PDMS ink before printing. Side-on and end-on projections reveal very straight and smooth features that are nearly round in cross section (Fig. 3A). Quantitative analysis of the 3D stacks demonstrates that the cross-sectional areas of printed features follow a simple conservation of volume equation, $A = Q/v$, where A is the feature's cross-sectional area, Q is the flow rate of the ink, and v is the translation speed of the nozzle (Fig. 3B). We also find that the features have a cross-sectional aspect ratio close to 1 across all flow rates and translation speeds. Thus, features between about 1 mm and 100 μm in diameter can be created by following this simple volume conservation law. Outside of this regime, features as small as 30 μm are generated by reducing the ink flow rate and increasing the nozzle translation speed, indicating the potential high level of precision that is possible with this 3D printing method.

We were intrigued by the accumulation of fluorescent particles at the interface between the printed PDMS structures and the supporting micro-organogel. We believe that this phenomenon is analogous to a well-known mechanism in which microphase-separated droplets are stabilized in an immiscible medium by microparticles or nanoparticles that become trapped at the fluid-fluid interface, reducing interfacial tension and preventing droplet coalescence (*33*, *34*). This phenomenon points to challenges that may arise in 3D printing PDMS inks that are formulated with nanoparticle fillers, which may inhibit adhesion between successive layers of printed structures. These effects do not occur

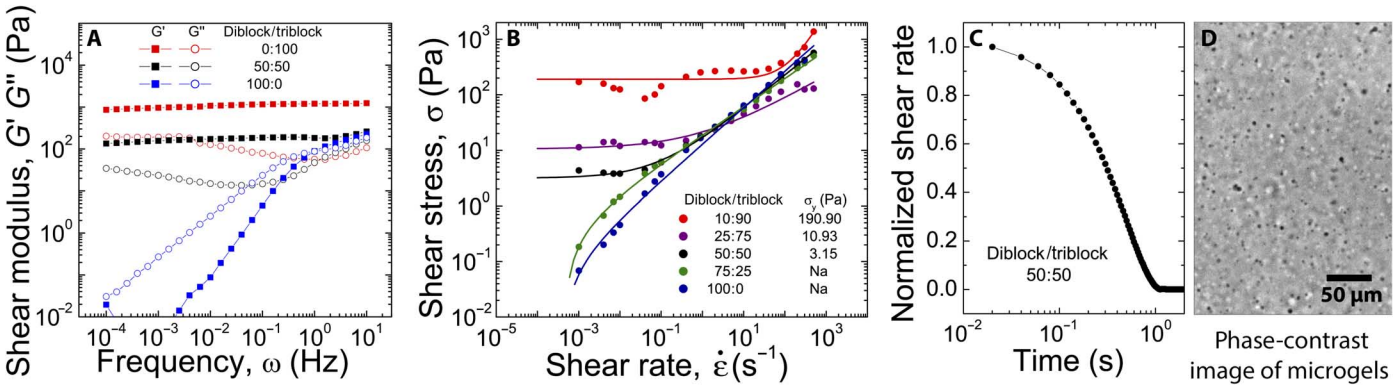

Fig. 2. Rheological characterization of block copolymer phases. The rheological properties, including frequency sweep (**A**) and yield stress (**B**) of block copolymer assemblies, are highly dependent on the ratio of diblock to triblock copolymers. At high diblock concentrations, the material demonstrates rheological properties associated with a liquid, including a crossover in the shear modulus at high frequencies and no determinable yield stress. At high triblock concentrations, the material shows rheological properties associated with an irreversibly cross-linked gel, including separated elastic and viscous shear modulus at high values and irrecoverable yielding at high stresses. Block copolymer blends show rheological properties favorable for 3D printing of soft materials, including separated elastic and viscous shear moduli with low elastic modulus, a low yield stress, and a fast recovery of elasticity after shearing. (**C**) Thixotropic response time of the block copolymer microgel system. (**D**) The samples exhibiting rheology suitable for 3D printing are found to be composed of 2- to 4-μm microgels, as seen in phase-contrast microscopy.

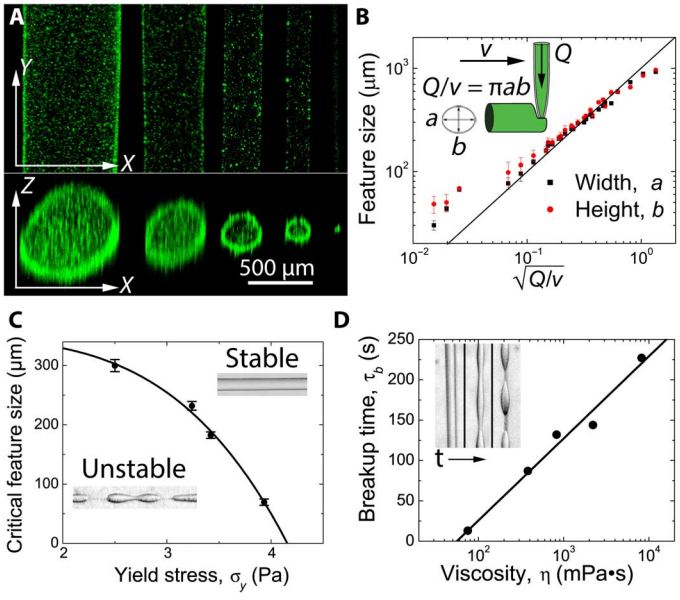

Fig. 3. Control of printed features. (**A**) The width and height of printed lines are measured using confocal microscopy at flow rates and tangential velocities of 5000 μl/hour at 2 mm/s, 5000 μl/hour at 10 mm/s, 1000 μl/hour at 3.5 mm/s, 1000 μl/hour at 10 mm/s, and 5 μl/hour at 6 mm/s. (**B**) Feature size of printed objects can be controlled by the tangential velocity of the nozzle (*v*) and the flow rate of the ink through the nozzle (*Q*). The printed feature size shows nearly ideal behavior across a wide range of velocities and flow rates. (**C**) The critical feature size in which neat silicone oil remains stable is controlled by the yield stress of the organogel; increasing the yield stress of the organogel decreases the critical feature size necessary to maintain stable features. (**D**) The time at which features printed below the critical feature size will begin to break up can be increased by increasing the shear viscosity of the silicone ink.

when printing with a miscible ink/support material pair, as the ink and support medium share a common solvent such as water. By contrast, the immiscible ink/support material pair used here creates a diffusion barrier and prevents this potential rapid molecular exchange between the ink and support material. This is a useful feature when the loss of chemical precursors from the ink into the support bath may interfere with processing steps after printing, such as photocrosslinking.

To estimate the strength of interaction between the organogel support material and the PDMS ink in the absence of added particulate fillers, we perform a series of interfacial and surface tension measurements with neat mineral oil and silicone oil. We measure the surface tension of silicone oil and mineral oil against air through the pendant drop method, finding that $\gamma_s = 19.0 \pm 0.9$ mN/m for silicone oil and $\gamma_m = 30.4 \pm 2.5$ mN/m for mineral oil, comparable to those reported in the literature (*35*, *36*). Stable hanging drops of silicone oil in a mineral oil bath were too small for reliable pendant drop measurements to be performed; increasing the size of the drop resulted in the silicone detaching from the needle before reaching an adequate size. Thus, to determine the interfacial tension between silicone oil and mineral oil, γ_{sm}, we place a drop of neat mineral oil on the silicone oil/air interface and measure the interfacial contact angles. Using these angle measurements and the surface tension measurements from the pendant drop, we solve Young's equation and find that $\gamma_{sm} = 13.1 \pm 2.2$ mN/m (see the Supplementary Materials).

To prevent the breakup of printed structures driven by interfacial instabilities, the stresses generated by interfacial tension must be less than the yield stress of the micro-organogel material (*31*, *37*). Thus, the minimum stable printed feature size may be controlled, in part, by the micro-organogel yield stress. We hypothesize that the minimum feature size can be predicted from a plastocapillary length, given by $\lambda = \gamma_{ms}/\sigma_y$. To test this relationship, we print features made from low-viscosity silicone oil into micro-organogels with different yield stresses and observe the feature stability over 24 hours. We find that the minimum stable feature size decreases with increasing yield stress, as predicted, although this back-of-the-envelope estimate does not quantitatively predict minimum feature size from our measurements of interfacial tension and yield stress (Fig. 3C). The block copolymer in the mineral oil phase may alter the interfacial tension with the silicone phase; thorough studies of the plastocapillary length that account for the added polymer must be performed in the future if quantitative predictions of minimum feature size are to be made (*31*, *38*). We find that the time until unstable feature breakup depends on the viscosity of the printed

material, revealing that even unstable features may be suitable for generating very fine, precise silicone structures if the curing time of the silicone is less than the time over which the interfacial instabilities dominate (Fig. 3D).

The interfacial tension between PDMS ink and the surrounding organogel support material is a driving force for feature instability, yet it also assists in creating 3D-printed parts with smooth surfaces. After 3D printing linear features made from Momentive UV Electro 225 PDMS and cross-linking through ultraviolet (UV) curing, we remove the cured part from the micro-organogel support material, clean it by serially washing it with solvents and surfactant solutions (see movie S3 and Materials and Methods), and characterize the surface in multiple ways. Scanning electron microscopy images reveal a very smooth surface (Fig. 4E), and scanning white light interferometry (SWLI) measurements demonstrate that printed parts have a surface roughness of 150 nm (Fig. 4, A to C). 3D-printed "dog-bone" parts designed to test mechanical strength are printed, cured, and removed from the organic support material by using the same protocols (Fig. 4F). Extensional stress-strain tests on dog-bone samples demonstrate excellent mechanical integrity of 3D-printed silicone parts, which fail at approximately 700% strain (see Fig. 4, D and G, and the Supplementary Materials). This physical robustness of the 3D-printed parts reveals that strong adhesion occurs between neighboring features during fabrication. To test whether layer-to-layer and lateral feature adhesion is achieved, we printed silicone sheets out of Momentive UV Electro 225 silicone in both the vertical and horizontal orientations. Both types of structures were found to be very robust, indicating good feature adhesion along both directions and enabling us to wash the structures and perform SWLI scans of their surfaces (see the Supplementary Materials).

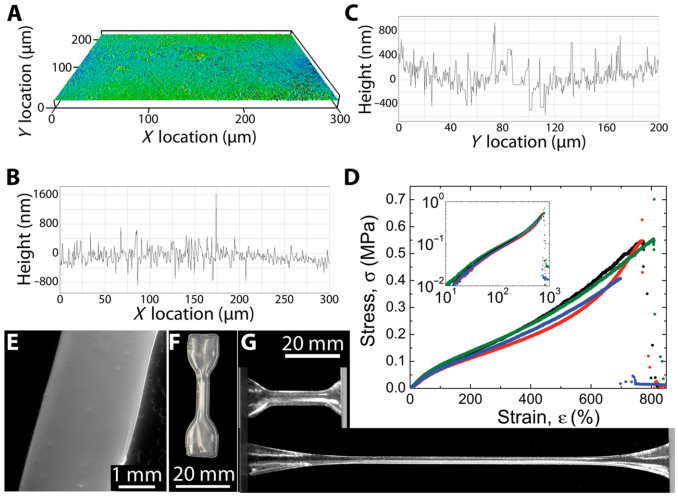

Fig. 4. Surfaces and mechanical properties of printed structures. (**A** to **C**) SWLI of a printed silicone surface shows a surface roughness of 150 nm [2D scan (A), slice along the *x* axis (B), and slice along the *y* axis (C)]. (**D**) Stress-strain curve of printed silicone dog-bone specimens; printed silicone structures are capable of enduring more than 700% strain before mechanical failure. Tensile tests maintain a linear stress-strain relationship at low strains (inset). (**E**) Scanning electron microscopy of the cross section of a printed silicone structure demonstrates the uniformity of printed structures. (**F**) Macrophotographic image of a dog-bone specimen printed from silicone elastomer for tensile testing. (**G**) Macrophotographic images of printed dog-bone structures in the relaxed and highly strained states.

Applications of 3D printing in micro-organogels

To explore the range of 3D printing capabilities enabled by the micro-organogel system, we print a variety of silicone elastomer structures with varying size, complexity, and materials. In one example, we print a model trachea implant with a wall thickness of 400 μm out of a room temperature vulcanizing (RTV) silicone, Mold Max 10, in which the diameter of the tube fluctuates with height (Fig. 5, A and B). After letting

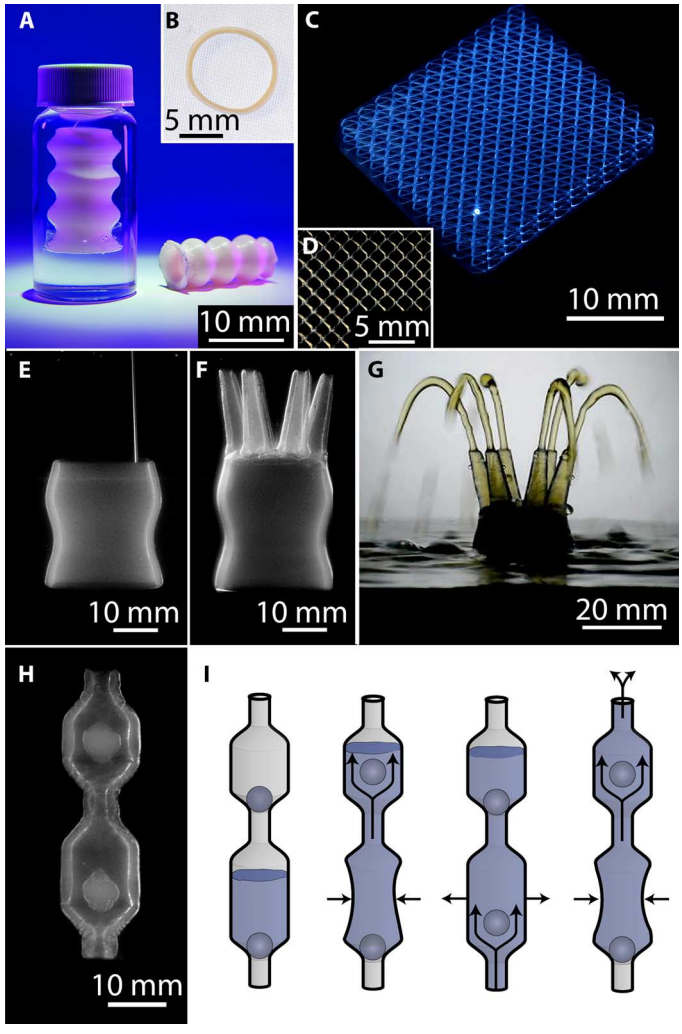

Fig. 5. Printed silicone structures. (**A**) Model trachea implants printed from RTV silicone elastomers into the micro-organogel support matrix retain their integrity and robustness once removed from the support material. (**B**) Cross section of the model trachea implant demonstrates the ability to print perfusable tubes with a wall thickness of 400 μm. (**C**) Silicone scaffold with sinusoidal wave pattern in both the *x-y* and *x-z* directions. (**D**) Top-down view of the silicone scaffold shows 250-μm-diameter features. (**E**) Macroscopic image of a perfusable network of hollow vessels being 3D-printed into the micro-organogel support material. (**F**) Macroscopic image of the completed, uncured silicone structure in the micro-organogel support material. The structure transitions from one large base with a diameter of 25 mm to six smaller tentacles with a diameter of 3 mm. (**G**) Once cured, the printed structure is removed from the organogel support material and cleaned. Fluid is pumped through the tubular network, demonstrating the capability of printed structure to support fluid flow. (**H**) Multiple parts are printed together to form a silicone pump with encapsulated ball valves supported by the micro-organogel material. (**I**) Scheme depicting the flow of fluid through the printed silicone pump. Applying repetitive compressive forces to the lower chamber pushes the fluid into the upper chamber and out the top of the pump.

the Mold Max 10 silicone cure at room temperature (25°C) for 24 hours, the model can be removed from the micro-organogel support material and handled. In a second example, we print a 20 mm × 20 mm × 8 mm 3D scaffold structure out of Momentive UV Electro 225 silicone, with sinusoidal wave patterns in both the *x*-*y* and *x*-*z* directions, with feature sizes on the order of 250 μm (Fig. 5, C and D). This structure was observed to be stable with time, indefinitely, but was made from features too thin to be removed from the medium and handled; improved methods to gently replace the micro-organogel material with low-viscosity solvents or other aqueous materials must be developed to handle these fine, delicate structures. To demonstrate the potential application of our method in challenging biomedical applications such as complex macroscale to mesoscale vasculature, we 3D-print a strong, flexible, perfusable, 3D network of hollow vessels out of Momentive UV Electro 225 silicone, in which a single 25-mm-diameter tube splits into six 3-mm-diameter vessels (Fig. 5, E and F). Once the structure is cured, removed from the micro-organogel support material, and cleaned, we are able to connect pipe fittings and pump fluids through all six openings at high flow rates (Fig. 5G and movie S4).

To demonstrate the ability to manufacture structures in the micro-organogel system with multiple encapsulated parts in a single step, we 3D-print a silicone pump out of Momentive UV Electro 225 silicone consisting of two ball valves to regulate the fluid motion. All three components of the silicone pump are 3D-printed as one continuous print job before they are cured and removed from the micro-organogel support material (Fig. 5H). After cleaning, fluid is pumped from the bottom chamber, through the upper chamber, and out the top by applying a compressive force to the lower chamber (Fig. 5I). The device is so physically robust that we are able to connect tubing to the tapered ends and pump fluid from one reservoir to another (see movie S5 and the Supplementary Materials).

DISCUSSION

Microgels have been used for many years as model systems to study the fundamental physics of the jamming and glass transitions (*6*, *8*, *10*). For an even longer period, dating back to the 1950s, microgels have been used in the industry to control the rheological behaviors of diverse products from engine oils to personal care products, such as lotions, shampoos, conditioners, and hand sanitizers (*3*, *39*–*41*). In contrast to aqueous microgels, organic microgel applications have remained limited by the challenges of microgel synthesis and swelling in nonpolar liquids. Here, we have developed an oil-based microgel system by leveraging one of the most well-controlled and versatile tools in the soft matter research world: the self-assembly of block copolymers. We used commercially available components and demonstrated the tunability of the material's rheological and interfacial properties. Our results demonstrate the ability of these microgels to meet the manufacturing requirements of soft silicone devices without significant constraints on ink formulation or fabrication machinery. Furthermore, we hope that this work will enable other researchers to investigate the huge diversity of possible block-copolymer chemistries, expanding the breadth of physical and chemical properties of micro-organogels for new technological applications, including improved soft matter manufacturing methods.

The minimum feature size, surface roughness of printed features, and the layer-to-layer spacing obtainable by printers are often used to describe the precision of rapid prototyping systems. Whereas the layer-to-layer spacing is driven by the mechanical precision of the printer, the minimum feature width and surface roughness are dependent on the material properties of the ink and support material; the appropriate measure of precision varies between different applications and the associated materials. Rapid prototyping systems are most frequently used to create large-scale, solid objects with marginal requirements for fine detail compared to precision machining (*42*, *43*), although increasing precision is a ubiquitous goal. Thus, silicone 3D printing systems that produce solid parts with feature size and a surface roughness of 1 mm are commercially available (*44*). The organic microgels developed here now bring this limit down by one to two orders of magnitude. This level of precision allows the fabrication of thin-walled tubes with a thickness of 450 μm that are robust enough to be handled and removed from the support material. Even smaller feature widths have been achieved, yet more robust materials and improved removal techniques are required if these delicate structures are to be removed from the support medium without failure.

3D bioprinting for tissue engineering has tremendous hurdles to overcome before implantable, functioning tissues and organs can be fabricated out of living cells (*45*). By contrast, 3D printing of implantable silicone devices is currently limited by the precision and strength of manufactured parts. The micro-organogel system developed here allows for the fabrication of devices suitable for biomedical applications that are robust enough to be handled, tested with standard industrial mechanical methods, and used in vigorous fluid pumping applications. The use of micro-organogel material to support printed parts allows multiple, nested components to be printed in a single step, opening the door for new methods and design strategies in additive silicone manufacturing. More generally, micro-organogels enable a wide breadth of potential applications where the unique rheology of the jamming transition is needed in oil-based systems.

MATERIALS AND METHODS

Preparing organogel support matrix

Organic microgels were prepared from the SEP copolymer S_{607}-*b*-EP_{1561} (molecular weight, 172.6 kg/mol; polydispersity, 1.03), consisting of 28 mole percent (mol %) polystyrene (KRATON G1702); the SEBS copolymer $S_{208.5}$-*b*-EB_{974}-*b*-$S_{208.5}$ (molecular weight, 98.1 kg/mol; polydispersity, 1.03), consisting of 30 mol % polystyrene (KRATON G1650); and light mineral oil [National Formulary/Food Chemicals Codex (NF/FCC)–grade] (Fisher Scientific). The various solubility parameters have been reported as 14.1, 17.1, 17.53, 16.2, and 20.1 $MPa^{1/2}$ for mineral oil, butylene, ethylene, propylene, and polystyrene, respectively (*46*, *47*). Block copolymer mixtures were prepared at 2.25 wt % diblock copolymer, 2.25 wt % triblock copolymer, and 95.5 wt % light mineral oil. Samples were heated to 150°C and continuously mixed using a Scilogex Overhead Stirrer set to 250 rpm for 4 to 6 hours. Other self-assembled phases were prepared by using the same protocols, but with the compositions specified in the manuscript body.

Preparing silicone elastomer inks

UV-curing silicone elastomer inks were prepared by mixing Momentive UV Electro 225 at a 50:1 base–to–curing agent ratio. Low-viscosity silicone oil (Sigma-Aldrich) was added at 25 wt % to lower the viscosity of the printing ink. Samples were homogeneously mixed at 3500 rpm for 30 s in a FlackTek DAC 150 SpeedMixer before they were degassed and loaded into a Hamilton GASTIGHT syringe. After printing, the silicone structures were cured under a 400-W, 320- to 390-nm UV flood curing lamp (Sunray) for 10 to 20 min. RTV silicone elastomer inks were prepared by mixing Smooth-On Mold Max 10 at a 10:1 base–to–

curing agent ratio. Samples were homogeneously mixed at 3500 rpm for 30 s in a speed mixer and loaded into a BD plastic syringe. After removal from the micro-organogel system, printed structures were washed first with warm soapy water (Alconox) and then with ethanol. Samples for testing feature size were printed using a UV-curing silicone elastomer formed from a vinyl-terminated PDMS base (Gelest DMS-V31) and a [2 to 3% (mercaptopropyl)methylsiloxane)]-dimethylsiloxane copolymer cross-linker (Gelest SMS-022) and were prepared at a 3:1 base–to–cross-linker ratio (gel fraction, 0.938). A stock solution of 2,2-dimethoxy-2-phenylacetophenone photoinitiator (Sigma-Aldrich) was prepared at 0.125 g/1 ml of ethanol and added to the vinyl-terminated silicone elastomer ink at 0.05 wt %. Finally, 1-μm fluorescent microspheres were added to the silicone elastomer ink at ~0.1 wt % for confocal imaging.

Silicone 3D printing

All 3D printing was performed using a linear stage as a syringe pump (Physik Instrumente) attached to three linear translation stages (Newport). Silicone elastomer inks were loaded into syringes equipped with either a disposable blunt dispensing needle (Vita Needle) or a custom-made glass needle. Glass needles were created by drawing a glass microcapillary (1 mm outer diameter) to a desired diameter using a pipette puller (David Kopf Instruments). Typical needle inner diameters vary over a range of 150 μm to 1 mm. Both the syringe pump and translation stages were controlled through custom-written MATLAB script functions and trajectory files.

Rheology

All rheological measurements were taken on a Malvern Kinexus pro+ rheometer using a roughened 40-mm upper cone with an angle of 4° and a roughened 40-mm lower plate. Frequency sweeps were taken at 1% strain from 10 to 10^{-4} Hz. The yield stress of the material was determined by applying a shear rate sweep from 500 to 10^{-3} s^{-1} and measuring the shear stress. The thixotropic time was measured by first applying a shear stress greater than the yield stress of the organic microgel system. The applied stress was then dropped below the yield stress of the material, and the shear rate was measured as a function of time.

Small-angle x-ray scattering

SAXS was performed using a Bruker NANOSTAR SAXS system. Samples were placed into quartz capillary tubes (diameter, 1.5 mm; wall thickness, 10 μm) and flame-sealed. SAXS measurements were taken over the course of 18 hours using a 2D wire detector with 1024 × 1024 pixels. The data were then integrated over the azimuthal angle.

Interfacial tension

Surface tensions were determined using the pendant drop method, in which a drop is suspended from a needle into air. Images of the droplet were taken and analyzed in MATLAB to determine the interfacial tension between the drop and air. Interfacial tension measurements between silicone oil and mineral oil were determined by measuring the contact angles formed by placing a drop of light mineral oil (NF/FCC-grade; Fisher Scientific) in a bath of 100 cSt oil (Sigma-Aldrich) and solving Young's equation. The contact angles were measured using FIJI ImageJ software.

Tensile test method

All tensile testing was performed using a six-axis load cell (AMTI), a linear variable differential transformer (LVDT) displacement transducer (RDP), and a ball-bearing slide (Parker). The test specimen was 3D-printed in accordance with ASTM D412 Type C specifications, with horizontal passes along its overall length. After curing, the tensile test specimen was clamped between the load cell and the LVDT. The slide was pulled to stretch the specimen until failure. The force and displacement were recorded with LabVIEW, and then stress and strain were calculated using the cross-sectional area and the length of the unstrained sample.

Gel permeation chromatography

Molecular weight and polydispersity were determined by gel permeation chromatography in tetrahydrofuran at 40°C and a flow rate of 1.0 ml/min (Agilent isocratic pump, degasser, and autosampler; columns: Waters Styragel 5-μm guard + two Waters Styragel HR 4E columns; molecular weight range, 101 to 2×10^5 g/mol). Detection consisted of an Agilent 1260 Infinity refractive index detector, and the system was calibrated using polystyrene standards.

Imaging

Photographs were taken using a Nikon D3X camera under bright-field illumination. Videos were recorded using a Nikon 7200 camera or an Imaging Source DMK 23GM021 camera under white light illumination. Micrographs were taken with a Nikon Eclipse Ti-E microscope with a C2 confocal scanning system. SWLI was performed using a Wyko NT9100 Optical Profiling System. Scanning electron microscopy was performed using a VEGA3 XMU scanning electron microscope.

SUPPLEMENTARY MATERIALS

Supplementary material for this article is available at http://advances.sciencemag.org/cgi/content/full/3/5/e1602800/DC1

fig. S1. Small-angle x-ray scattering.
fig. S2. Rheological measurements.
fig. S3. Effects of elevated temperature on rheological properties.
fig. S4. Measuring interfacial tension using the pendant drop method and contact angles.
fig. S5. Loading and unloading stress-strain curves.
fig. S6. Layer-to-layer and lateral adhesion between printed filaments.
movie S1. Phase-contrast microscopy of dilute sample.
movie S2. 3D printing a model trachea.
movie S3. Removal of a cured silicone structure.
movie S4. Fluid flow through a 3D-printed perfusable tube network.
movie S5. Fluid pumped through a 3D-printed silicone valve.

REFERENCES AND NOTES

1. J. A. Bonham, M. A. Faers, J. S. van Duijneveldt, Non-aqueous microgel particles: Synthesis, properties and applications. *Soft Matter* **10**, 9384–9398 (2014).
2. D. Saatweber, B. Vogt-Birnbrich, Microgels in organic coatings. *Prog. Org. Coat.* **28**, 33–41 (1996).
3. B. R. Saunders, B. Vincent, Microgel particles as model colloids: Theory, properties and applications. *Adv. Colloid Interface Sci.* **80**, 1–25 (1999).
4. J. B. Thorne, G. J. Vine, M. J. Snowden, Microgel applications and commercial considerations. *Colloid Polym. Sci.* **289**, 625–646 (2011).
5. D. F. Evans, H. Wennerstrom, *The Colloidal Domain* (Wiley-Vch, 1999).
6. D. Bi, J. Zhang, B. Chakraborty, R. P. Behringer, Jamming by shear. *Nature* **480**, 355–358 (2011).
7. P. Coussot, L. Tocquer, C. Lanos, G. Ovarlez, Macroscopic vs. local rheology of yield stress fluids. *J. Non-Newton. Fluid Mech.* **158**, 85–90 (2009).
8. A. J. Liu, S. R. Nagel, Nonlinear dynamics: Jamming is not just cool any more. *Nature* **396**, 21–22 (1998).
9. P. Menut, S. Seiffert, J. Sprakel, D. A. Weitz, Does size matter? Elasticity of compressed suspensions of colloidal-and granular-scale microgels. *Soft Matter* **8**, 156–164 (2012).
10. C. Pellet, M. Cloitre, The glass and jamming transitions of soft polyelectrolyte microgel suspensions. *Soft Matter* **12**, 3710–3720 (2016).

11. T. Bhattacharjee, C. J. Gil, S. L. Marshall, J. M. Urueña, C. S. O'Bryan, M. Carstens, B. G. Keselowsky, G. D. Palmer, S. Ghivizzani, C. P. Gibbs, Liquid-like solids support cells in 3D. *ACS Biomater. Sci. Eng.* **2**, 1787–1795 (2016).
12. T. Bhattacharjee, S. M. Zehnder, K. G. Rowe, S. Jain, R. M. Nixon, W. G. Sawyer, T. E. Angelini, Writing in the granular gel medium. *Sci. Adv.* **1**, e1500655 (2015).
13. T. J. Hinton, A. R. Hudson, K. Pusch, A. Lee, A. W. Feinberg, 3D printing PDMS elastomer in a hydrophilic support bath via freeform reversible embedding. *ACS Biomater. Sci. Eng.* **2**, 1781–1786 (2016).
14. P. J. Flory, *Principles of Polymer Chemistry* (Cornell Univ. Press, 1953).
15. M. Morton, *Rubber Technology* (Springer, 2013).
16. K. E. Polmanteer, Silicone rubber, its development and technological progress. *Rubber Chem. Technol.* **61**, 470–502 (1988).
17. N. Bhattacharjee, A. Urrios, S. Kang, A. Folch, The upcoming 3D-printing revolution in microfluidics. *Lab Chip* **16**, 1720–1742 (2016).
18. B. Derby, Inkjet printing of functional and structural materials: Fluid property requirements, feature stability, and resolution. *Annu. Rev. Mat. Res.* **40**, 395–414 (2010).
19. J. Stringer, B. Derby, Formation and stability of lines produced by inkjet printing. *Langmuir* **26**, 10365–10372 (2010).
20. T. Femmer, A. J. C. Kuehne, M. Wessling, Print your own membrane: Direct rapid prototyping of polydimethylsiloxane. *Lab Chip* **14**, 2610–2613 (2014).
21. M. S. Mannoor, Z. Jiang, T. James, Y. L. Kong, K. A. Malatesta, W. O. Soboyejo, N. Verma, D. H. Gracias, M. C. McAlpine, 3D printed bionic ears. *Nano Lett.* **13**, 2634–2639 (2013).
22. P. Alexandridis, U. Olsson, B. Lindman, A record nine different phases (four cubic, two hexagonal, and one lamellar lyotropic liquid crystalline and two micellar solutions) in a ternary isothermal system of an amphiphilic block copolymer and selective solvents (water and oil). *Langmuir* **14**, 2627–2638 (1998).
23. F. S. Bates, G. Fredrickson, Block copolymers—Designer soft materials. *Phys. Today* **52**, 32–38 (1999).
24. Y. R. Sliozberg, K. E. Strawhecker, J. W. Andzelm, J. L. Lenhart, Computational and experimental investigation of morphology in thermoplastic elastomer gels composed of AB/ABA blends in B-selective solvent. *Soft Matter* **7**, 7539–7551 (2011).
25. A. Halperin, Polymeric micelles: A star model. *Macromolecules* **20**, 2943–2946 (1987).
26. D. Izzo, C. M. Marques, Formation of micelles of diblock and triblock copolymers in a selective solvent. *Macromolecules* **26**, 7189–7194 (1993).
27. J. H. Laurer, R. Bukovnik, R. J. Spontak, Morphological characteristics of SEBS thermoplastic elastomer gels. *Macromolecules* **29**, 5760–5762 (1996).
28. K. Mortensen, Structural properties of self-assembled polymeric micelles. *Curr. Opin. Colloid Interface Sci.* **3**, 12–19 (1998).
29. K. J. LeBlanc, S. R. Niemi, A. I. Bennett, K. L. Harris, K. D. Schulze, W. G. Sawyer, C. Taylor, T. E. Angelini, Stability of high speed 3D printing in liquid-like solids. *ACS Biomater. Sci. Eng.* **2**, 1796–1799 (2016).
30. W. H. Herschel, R. Bulkley, Konsistenzmessungen von gummi-benzollösungen. *Colloid Polym. Sci.* **39**, 291–300 (1926).
31. E. Pairam, H. Le, A. Fernández-Nieves, Stability of toroidal droplets inside yield stress materials. *Phys. Rev. E* **90**, 021002 (2014).
32. J. C. Maxwell, On the calculation of the equilibrium and stiffness of frames. *London Edinburgh Dublin Philos. Mag. J. Sci.* **27**, 294–299 (1864).
33. B. P. Binks, Particles as surfactants—Similarities and differences. *Curr. Opin. Colloid Interface Sci.* **7**, 21–41 (2002).
34. S. U. Pickering, CXCVI.—Emulsions. *J. Chem. Soc. Trans.* **91**, 2001–2021 (1907).
35. C. A. Stan, S. K. Y. Tang, G. M. Whitesides, Independent control of drop size and velocity in microfluidic flow-focusing generators using variable temperature and flow rate. *Anal. Chem.* **81**, 2399–2402 (2009).
36. W. R. Jones Jr., L. D. Wedeven, "Surface-tension measurements in air of liquid lubricants to 200° C by the differential-maximum-bubble-pressure technique" (NASA TN D-6450, *NASA* 1971); https://ntrs.nasa.gov/archive/nasa/casi.ntrs.nasa.gov/19710024039.pdf.
37. H. Mehrabian, J. J. Feng, Capillary breakup of a liquid torus. *J. Fluid Mech.* **717**, 281–292 (2013).
38. R. W. Style, L. Isa, E. R. Dufresne, Adsorption of soft particles at fluid interfaces. *Soft Matter* **11**, 7412–7419 (2015).
39. B. W. Barry, M. C. Meyer, The rheological properties of carbopol gels II. Oscillatory properties of carbopol gels. *Int. J. Pharm.* **2**, 27–40 (1979).
40. J.-Y. Kim, J.-Y. Song, E.-J. Lee, S.-K. Park, Rheological properties and microstructures of Carbopol gel network system. *Colloid Polym. Sci.* **281**, 614–623 (2003).
41. A. K. Singla, M. Chawla, A. Singh, Potential applications of carbomer in oral mucoadhesive controlled drug delivery system: A review. *Drug Dev. Ind. Pharm.* **26**, 913–924 (2000).
42. H. N. Chia, B. M. Wu, Recent advances in 3D printing of biomaterials. *J. Biol. Eng.* **9**, 4 (2015).
43. S. V. Murphy, A. Atala, 3D bioprinting of tissues and organs. *Nat. Biotechnol.* **32**, 773–785 (2014).
44. Printing with Silicones: Building 3D Objects Layer by Layer (Walker Inc., 2015); http://www.wacker.com/cms/media/en/documents/feature-pdf/3d_druck.pdf.
45. J. S. Miller, The billion cell construct: Will three-dimensional printing get us there? *PLOS Biol.* **12**, e1001882 (2014).
46. T. L. Chantawansri, A. J. Duncan, J. Ilavsky, K. K. Stokes, M. C. Berg, R. A. Mrozek, J. L. Lenhart, F. L. Beyer, J. W. Andzelm, Phase behavior of SEBS triblock copolymer gels. *J. Polym. Sci. B* **49**, 1479–1491 (2011).
47. J. H. Laurer, S. A. Khan, R. J. Spontak, M. M. Satkowski, J. T. Grothaus, S. D. Smith, J. S. Lin, Morphology and rheology of SIS and SEPS triblock copolymers in the presence of a midblock-selective solvent. *Langmuir* **15**, 7947–7955 (1999).

Acknowledgments: We thank A. Fernandez-Nieves for sharing his expertise in granular yield stress materials. We also thank E. Dufresne and J. Burdick for their thoughtful and helpful comments. **Funding:** This work was funded by the NSF under grant number DMR-1352043. **Author contributions:** T.E.A. and W.G.S. first conceived this project and provided supervision and guidance. C.S.O. developed the micro-organogel and confirmed the presence of jammed microgels through SAXS and phase-contrast microscopy. In addition, C.S.O. performed feature size measurements, silicone ink stability measurements, interfacial tension measurements, and surface roughness measurements. K.D.S. performed interfacial tension measurements. C.S.O. and T.B. first printed silicone structures into micro-organogels. S.H. printed dog-bone specimens and performed tensile test measurements. C.P.K. and B.S.S. measured the molecular weight of the block copolymers and assisted in characterizing the micro-organogels. I.C. measured rheological properties of organogels prepared at varying polymer concentrations. C.S.O. and T.E.A. wrote the manuscript. **Competing interests:** A provisional patent titled "Organic microgel system for 3D printing of silicone structures" (serial number 62/382,652) was filed by T.E.A., B.S.S., C.S.O., W.G.S., and T.B. on 1 September 2016 and has been acknowledged by the U.S. Patent office. This patent was applied for by the University of Florida Research Foundation Inc. (Gainesville, FL). All other authors declare that they have no competing interests. **Data and materials availability:** All data needed to evaluate the conclusions in the paper are presented in the paper and/or the Supplementary Materials. Additional data related to this paper may be requested from the authors.

Submitted 11 November 2016
Accepted 9 March 2017
Published 10 May 2017
10.1126/sciadv.1602800

Citation: C. S. O'Bryan, T. Bhattacharjee, S. Hart, C. P. Kabb, K. D. Schulze, I. Chilakala, B. S. Sumerlin, W. G. Sawyer, T. E. Angelini, Self-assembled micro-organogels for 3D printing silicone structures. *Sci. Adv.* **3**, e1602800 (2017).

ScienceAdvances
AAAS

Self-assembled micro-organogels for 3D printing silicone structures

Christopher S. O'Bryan, Tapomoy Bhattacharjee, Samuel Hart, Christopher P. Kabb, Kyle D. Schulze, Indrasena Chilakala, Brent S. Sumerlin, W. Gregory Sawyer and Thomas E. Angelini (May 10, 2017)

Sci Adv 2017, 3:.
doi: 10.1126/sciadv.1602800

Science Advances

AAAS

advances.sciencemag.org/cgi/content/full/3/5/e1602800/DC1

Supplementary Materials for

Self-assembled micro-organogels for 3D printing silicone structures

Christopher S. O'Bryan, Tapomoy Bhattacharjee, Samuel Hart, Christopher P. Kabb, Kyle D. Schulze, Indrasena Chilakala, Brent S. Sumerlin, W. Gregory Sawyer, Thomas E. Angelini

Published 10 May 2017, *Sci. Adv.* **3**, e1602800 (2017)
DOI: 10.1126/sciadv.1602800

The PDF file includes:

Other Supplementary Material for this manuscript includes the following:
(available at advances.sciencemag.org/cgi/content/full/3/5/e1602800/DC1)

- movie S1 (.mov format). Phase-contrast microscopy of dilute sample.
- movie S2 (.mov format). 3D printing a model trachea.
- movie S3 (.mov format). Removal of a cured silicone structure.
- movie S4 (.mov format). Fluid flow through a 3D-printed perfusable tube network.
- movie S5 (.mov format). Fluid pumped through a 3D-printed silicone valve.

Small Angle X-Ray Scattering

Small angle X-ray scattering in conjunction with stoichiometric calculations provide us with insight into the micro- and nano-structure of our organogel systems. We estimate the number of copolymer chains present in a single unit core by multiplying the polymer chain density of the organogel system by the volume of a unit cell. In order to determine the volume of a unit cell, we perform small angle X-ray scattering measurements on organogel samples prepared at a global polymer concentration of 4.5 wt% consisting of 100% diblock copolymer, 100% triblock copolymer or an equal blend of the two (fig. S1). By determining the location of the first peak in scattering intensity, $S(q)$, located at $q = q_1$, we are able to calculate the average core to core spacing, d, for each sample, $d = 2\pi / q_1$. With the core to core spacing, we can estimate the volume of each unit cell as $= 4\pi d^3/24$. To determine the polymer chain density of the organogel system, we divide the total number of chains by the total volume. We estimate the total number of chains present in the organogel system by taking into consideration the total molecular weight of the block copolymer chains, the molecular weights of styrene, ethylene/butylene, and ethylene/propylene, and the composition of the polymers as provided by the manufacturer. We use gel permeation chromatography (GPC) to calculate the molecular weight of the triblock and diblock copolymers. We find the molecular weight of the KRATON G1650 triblock copolymer to be 98.1 kg/mol and the molecular weight of the KRATON G1702 diblock copolymer to be 172.6 kg/mol. The total volume of the organogel system is calculated from the mass quantities and densities of the block copolymers and mineral oil present in the system. We find the pure triblock organogel consists of ~12 triblock chains/unit cell core; the pure diblock organogel consists of ~6 diblock chains/unit cell core; and the blended organogel consists of ~6 triblock chains and ~3-4 diblock chains/unit cell core.

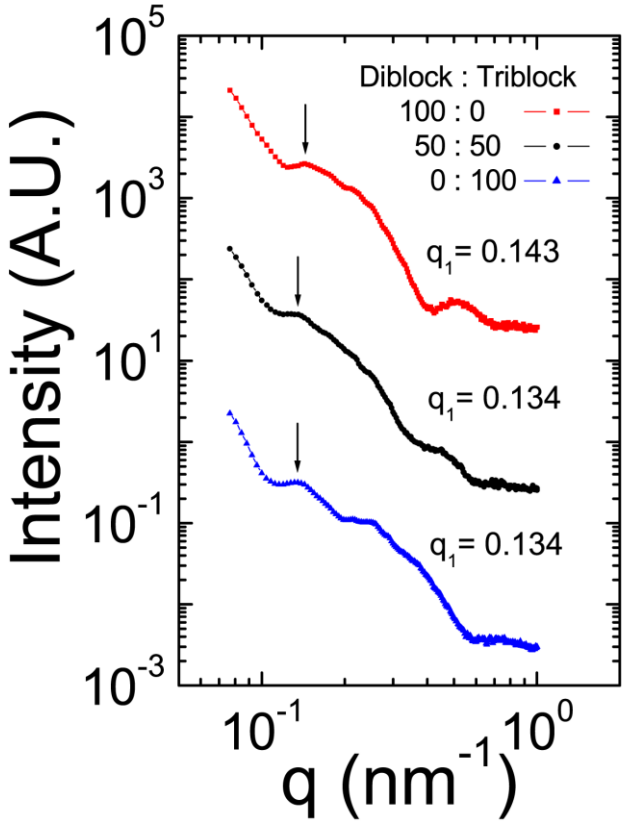

fig. S1. Small-angle x-ray scattering. Small angle X-ray scattering data showing the locations of the first peaks for self-assembled phases prepared at 4.5 wt% global polymer concentration at different ratios of diblock and triblock copolymers.

Rheological Measurements

Rheological properties of the organo-microgel system can be controlled by changing the relative concentration of diblock and triblock copolymer (Fig. 2), and by adjusting the overall global polymer concentration. Decreasing the global polymer concentration results in both a decrease in the yield stress of the organogel system (fig. S2B) as well as a decrease in the elastic shear modulus (fig. S2A). Below a 3 wt% global polymer concentration, the sample no longer exhibits rheological properties associated with a jammed micro-organogel system. As one of several checks to test whether the material is a microgel system, we compare the yield stress (fig. S2C) and frequency response (fig. S2D) of the micro-organogel both before and after the application of a steady, unidirectional shear at a rate of 500 s^{-1}. We find that the post-shear yield stress, elastic modulus, and viscous modulus are identical to those found before shearing, demonstrating that the sample behavior is consistent with a jammed microgel system and inconsistent with a crosslinked network.

The ability of micro-organogel material to be used as support material in silicone 3D printing is independent of the silicone ink used. We have demonstrated printing with several different silicone inks including neat silicone, room temperature vulcanization silicone elastomers (Mold Max and Sylgard), and UV curing silicone elastomers (Momentive). The shear viscosities of the silicone inks have ranged from from 10 to 100,000 mPa s (fig. S2E).

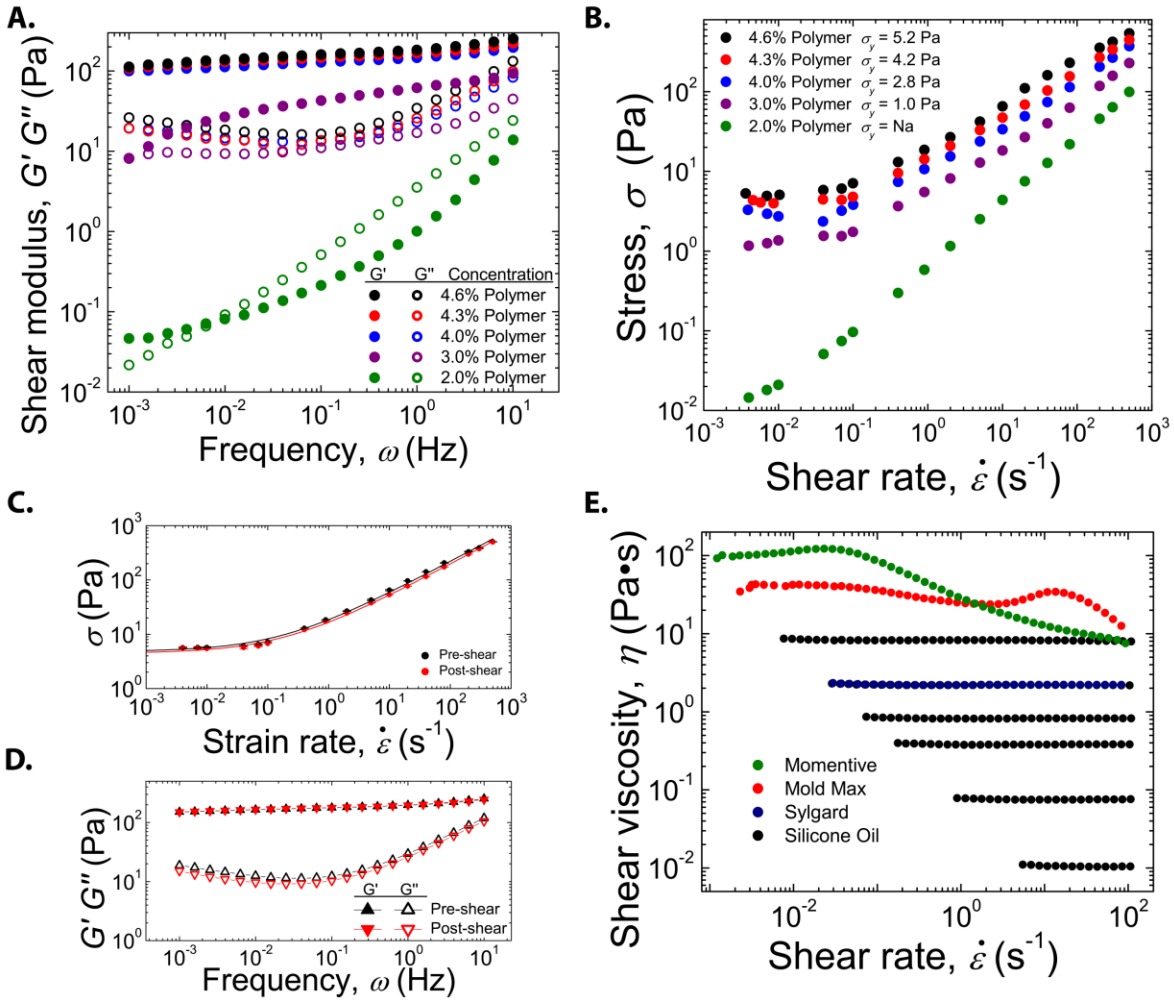

fig. S2. Rheological measurements. (**A**) Frequency sweep response, including the elastic and viscous shear moduli of organogel samples prepared across a range of global polymer concentrations. (**B**) Yield stress measurements of organogel samples prepared across a range of global polymer concentrations. (**C**, **D**) Micro-organogel samples show identical yield stress and frequency sweep responses before and after a unidirectional shear applied for 5 minutes at a rate of 500 s^{-1}, indicating the material is not a crosslinked network, but rather a jammed microgel system. (**E**) Shear viscosities of various silicone inks printed into the micro-organogel system.

Effects of Temperature

To explore the applicability of the micro-organogel support material for 3D printing silicones requiring high temperature curing, we investigate the effects of elevated temperatures on its rheological properties. The shear moduli of the micro-organogel are measured at 1Hz and 1% strain for temperatures between 25°C and 80°C. We observe a crossover in the elastic and shear modulus between 60°C and 70°C (fig. S3A). To further investigate the material properties as a function of temperature, we perform frequency sweeps at 1% strain and yield stress measurements for gels heated to 50°C, 60°C, and 70°C (fig. S3, B and C). The micro-organogel loses all signatures of elastic solids and exhibits no yield stress at 60°C and higher. This transition from a Herschel-Bulkley yield stress material to non-Newtonian fluid at elevated temperature could potentially be exploited in the removal of printed features from the micro-organogel support material.

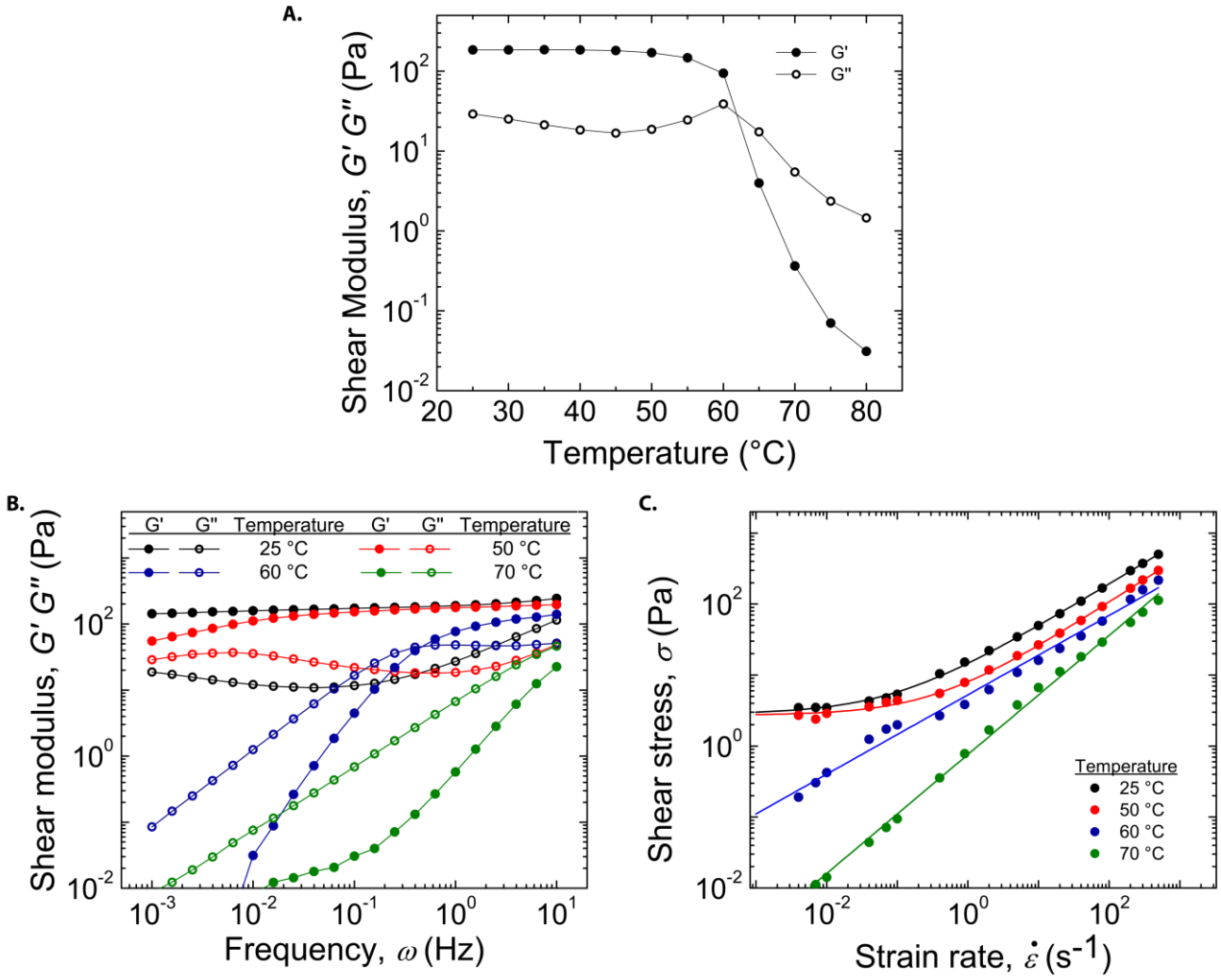

fig. S3. Effects of elevated temperature on rheological properties. (**A**) Micro-organogels heated to 60°C and higher behave as non-Newtonian viscous fluids, exhibiting a crossover in the elastic and viscous shear moduli. Measurements taken at 1 Hz and 1% strain. (**B**) At 50°C, the elastic modulus continues to dominate the viscous modulus; at 60°C, we find a crossover in the moduli and the viscous modulus begins to dominate at low frequencies. (**C**) We find similar results in the yield stress of the material; the yield stress remains relatively unchanged for temperatures up to 50°C, but no discernable yield stress for materials heated to 60°C and higher.

Interfacial Tension

We employ the pendant drop method to measure the interfacial tension across various interfaces, including neat silicone oil and mineral oil. In order to define the interface between the drop and surrounding material, an image of the drop is captured in front of a diffuse light source (fig. S4A). The location of the drop edge is determined with high confidence and precision by fitting an error function to radial slices of image intensity (fig. S4B). Once defined, the edge location is converted to Cartesian coordinates and we fit moving circular arcs to the local neighborhoods of each data point to smooth the shape of the drop, determine the local radius of curvature, and determine the local angle formed with the x-axis (fig. S4C). We calculate the interfacial tension for each location along the droplet using the Young-Laplace equation, $1/(\mathrm{R}/\mathrm{a}) + \sin\phi/(x/a) = -B(\mathrm{z}/\mathrm{a}) + 2$, where R is the radius of curvature at location (x,z), a is the radius of curvature at the origin (0,0), $\sin\phi$ is the angle between the tangent to the drop at x,z and the x-axis, and B is defined as $B = a^2 g\Delta\rho/\gamma$, where g is the gravitational constant, $\Delta\rho$ is the difference in density between the drop and the support bath, and γ is the interfacial tension. To eliminate outlying values resulting from extreme solutions to the Young-Laplace equation (e.g. when x = 0), we plot the calculated interfacial tension values from smallest to largest and remove the extreme values from consideration (fig. S4D). The average of the remaining values is calculated to determine the interfacial tension between the drop and the support bath (fig. S4F). We find the interfacial tension measurements for the water-air, mineral oil-air, and silicone oil-air interfaces are comparable to those found in the literature.

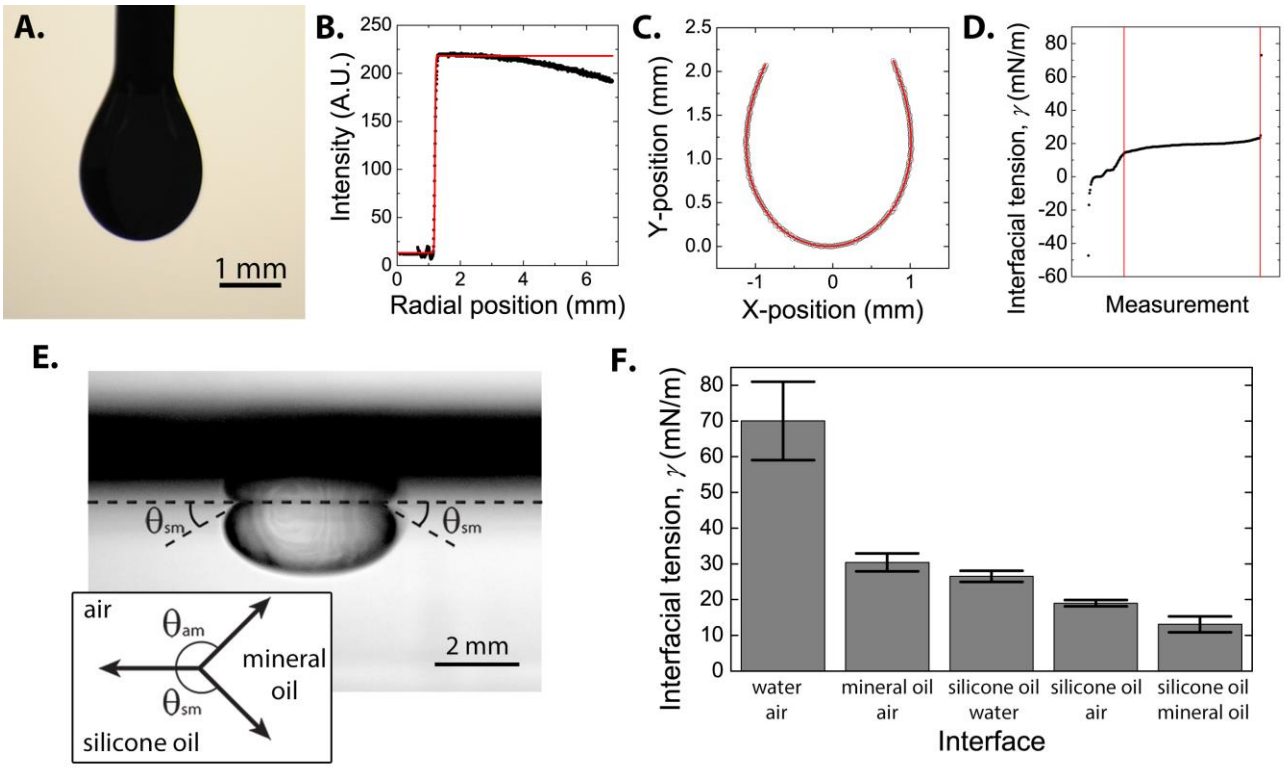

fig. S4. Measuring interfacial tension using the pendant drop method and contact angles. (**A)** Interfacial tension measurements are taken using the pendant drop method in which a drop is placed in front of a diffuse light source to create a well-defined edge. (**B**) An error function is fit to the intensity to determine the location of the drop edge. (**C**) We fit the Young-Laplace equation to the curve to determine the interfacial tension for each point along the curve. (**D**) Interfacial tension measurements are plotted from smallest to largest and extreme values are removed from consideration. (**E**) Contact angle measurements of a mineral oil drop placed in a silicone oil bath. The horizontal dashed line lays on the oil-air interface; the apparent object above this line is a reflection that arises from imaging the droplet from a grazing angle below the horizon.

We find that θ_{am} is approximately π. (**F**) Interfacial tension values calculated from solving Young's equation and from pendant drop analysis.

Mechanical Integrity of Printed Structures

We investigate the mechanical integrity of 3D printed silicone parts through extensional stress-strain tests on 3D printed 'dog-bones'. Printed specimens extended to 100% strain and subsequently relaxed follow nearly identical loading and unloading curves (fig. S5A). Similarly, the loading and unloading curves for samples extended to 600% strain align as well (fig. S5B). Furthermore, the stress-strain relationship for both the 100% and the 600% samples appear linear until ~60% strain (fig. S5, C and D).

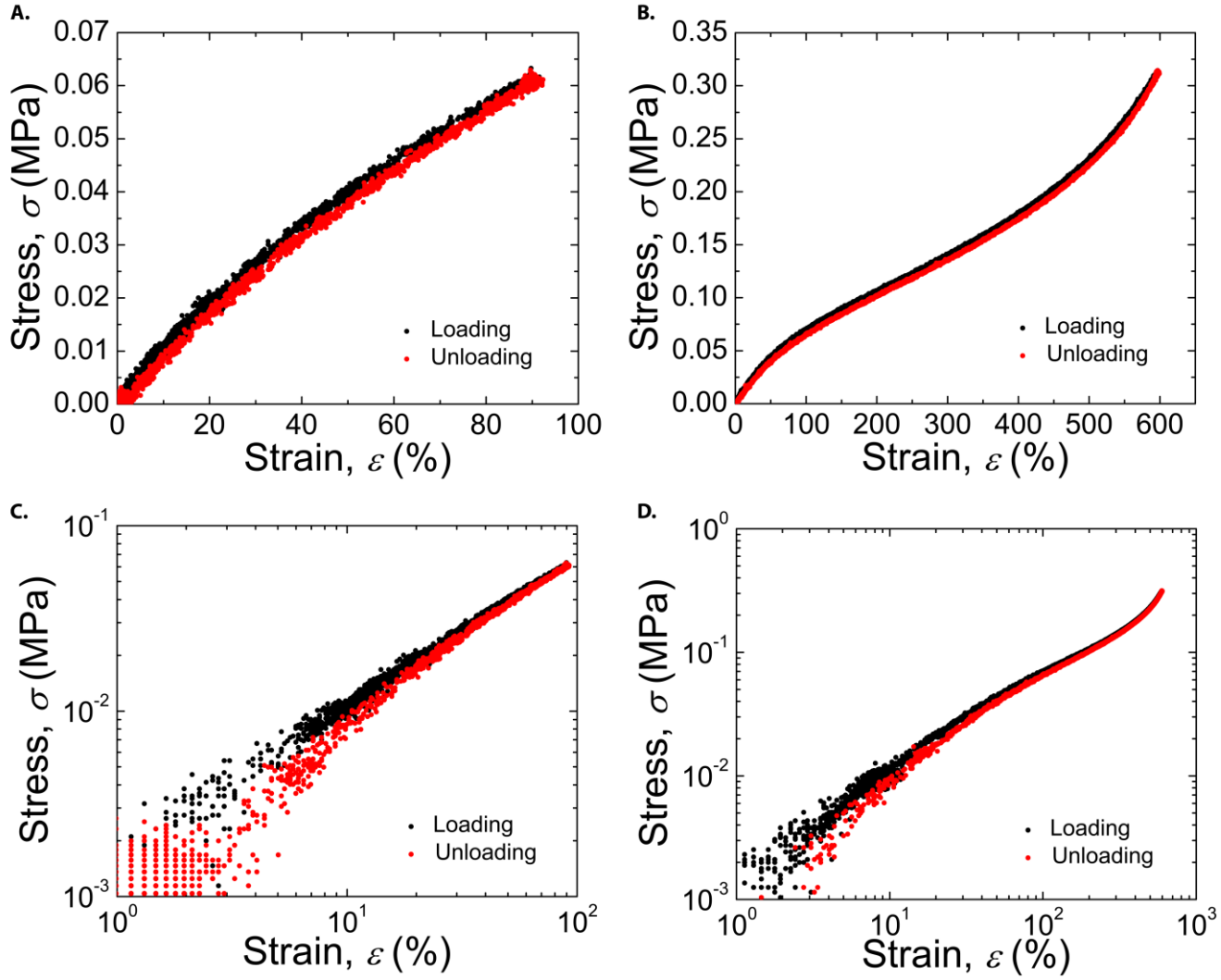

fig. S5. Loading and unloading stress-strain curves. (**A**) Dogbone specimens stretched to 100% strain follow nearly identical loading and unloading curves. (**B**) 'Dogbone' specimens stretched to 600% strain continue to follow nearly identical loading and unloading curves. (**C**, **D**) Both the 100% strain and 600% strain samples maintain linearity up to ~60% strain.

Adhesion Between Layers

Strong adhesion between printed filaments in both the vertical and lateral direction is necessary for printing mechanically robust silicone structures. To investigate the lateral adhesion between printed filaments, we printing a horizontal sheet of silicone in the x-y plane (fig. S6, A and B). The printed sheet is cured and removed from the micro-organogel support with no visual defects. SWLI scans of the surface show full adhesion between printed filaments (fig. S6C). To investigate the vertical layer-to-layer adhesion of printed features, we print a vertical sheet of silicone in the x-z plane (fig. S6, D and E). Once cured, we remove the sheet from the support bath and find adhesion between layers is obtained. We observe ridges on the surface of the vertical sheet that appear to correspond to the individual print layers. SWLI scans of the surface show several sharp valleys corresponding to the location of void pixels (fig. S6F). These void pixels typically occur in SWLI scans in narrow valleys.

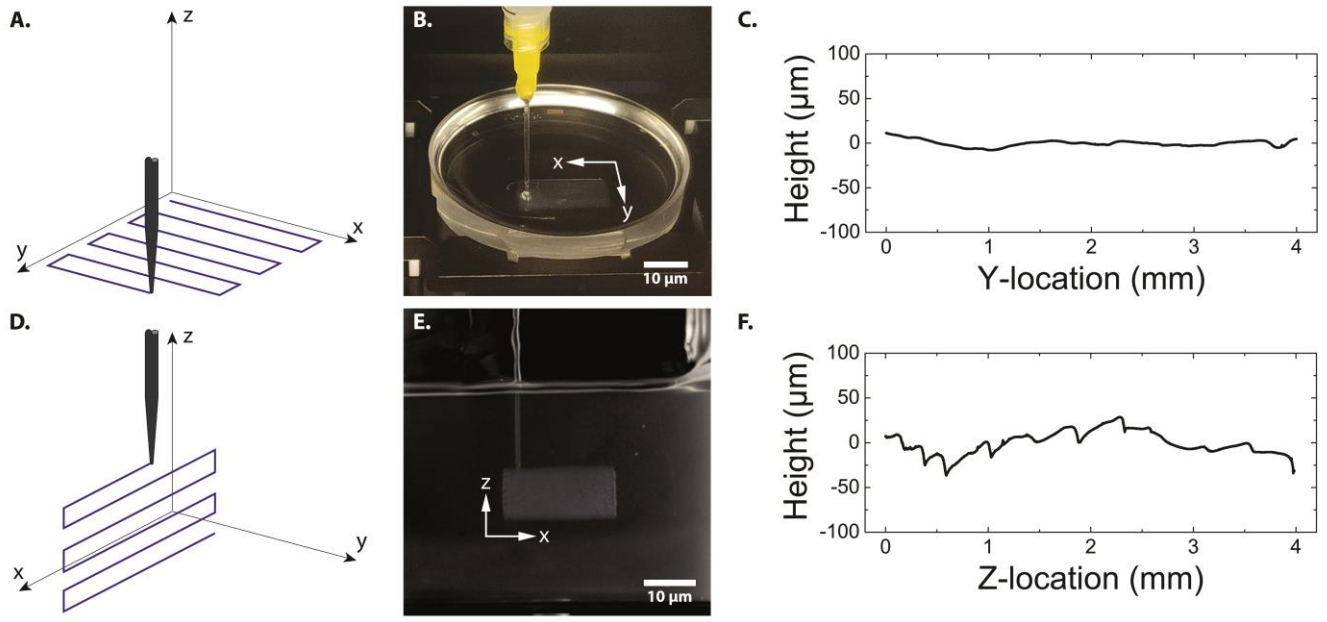

fig. S6. Layer-to-layer and lateral adhesion between printed filaments. (**A**) Horizontal silicone sheets are printed in the x-y plane to explore lateral adhesion between extruded filaments. (**B**) Macroscopic image of the horizontal sheet being printed into the micro-organogel material. (**C**) SWLI scans along the y-direction of the horizontal sheet. (**D**) Vertical silicone sheets are printed in the x-z plane to explore layer-to-layer adhesion of printed structures. (**E**) Macroscopic image of the vertical sheet being printed into the micro-organogel material. (**F**) SWLI scans along the z-direction of the vertical sheet.

movie S1. Phase-contrast microscopy of dilute sample.

movie S2. 3D printing a model trachea.

movie S3. Removal of a cured silicone structure.

movie S4. Fluid flow through a 3D-printed perfusable tube network.

movie S5. Fluid pumped through a 3D-printed silicone valve.